Available online at www.sciencedirect.com
ScienceDirect
Trans. Nonferrous Met. Soc. China 29(2019) 1323−1331
Transactions of Nonferrous Metals Society of China
www.tnmsc.cn

# Effect of lithium ion on seed precipitation from sodium aluminate solution

Wen-qiang HUANG, Gui-hua LIU, Jin-bin JU, Xiao-bin LI, Qiu-sheng ZHOU, Tian-gui QI, Zhi-hong PENG

School of Metallurgy and Environment, Central South University, Changsha 410083, China

Received 11 June 2018; accepted 12 November 2018

**Abstract:** Effect of lithium ion in sodium aluminate solution on precipitation rate, lithium content, morphology, and crystallization of alumina trihydrate (ATH) was investigated. Results showed that increasing lithium ion concentration in solution improved the precipitation rate and lithium content in ATH, whereas reduced the mass fraction of lithium precipitation from solution. Lithium ion in solution generated the fine ATH, and thereafter significantly increased the total particle number due to the preferential nucleation. Elevating temperature or reducing lithium ion concentration decreased lithium content in ATH and reduced the fine particle amount. Moreover, lithium ion in the solution changed the morphology of ATH by improving the growth of the (110) and (200) planes of gibbsite. A large amount of fine bar- or flake-shaped ATH attached on the coarse particles also benefited the secondary nucleation and led to the poor strength of alumina. All results will further contribute to improving the quality of alumina.

**Key words:** lithium; sodium aluminate solution; seed precipitation; alumina trihydrate

## 1 Introduction

Lithium extensively occurs in bauxite [1−4]. Accordingly, lithium is found in the pregnant sodium aluminate solution, alumina trihydrate (ATH), alumina and red mud [5]. Lithium-rich alumina, from calcined lithium-rich ATH, excessively increases lithium content in molten electrolytes (LiF 4−8 wt.%) during aluminum electrolysis [6,7], and thereafter the remarkable decrease in current efficiency occurs [7,8]. As lithium precipitation in precipitation of ATH from aluminate solution gives rise to lithium-rich alumina, alumina quality depends on lithium co-precipitated with ATH. Hence, the effect of lithium ion in solution on ATH precipitation should be illustrated clearly.

Li, Na, K and Cs are alkali elements, of which the solubility of $Li^+$ ion in aluminate solution is significantly less than that of $Na^+$ and $K^+$ ions [9,10]. By contrast, the effect of $K_2O$ on seed precipitation was extensively studied in sodium aluminate solution [11−15]. Presence of $K^+$ ion ($K_2O$ 10−90 g/L) in aluminate solution slightly improved precipitation rate and ratio. Meanwhile, morphology of gibbsite was different from that precipitated from the pure sodium aluminate solution. In addition, LEE et al [16] found that gibbsite was precipitated in hexagonal prism in the presence of potassium and caesium. However, few works are available regarding ATH precipitated from sodium aluminate solution containing lithium ion. XU et al [17] proposed an effective attempt to remove lithium ions from the Bayer liquor by the layered $H_2TiO_3$-type lithium ion sieves (LISs), while the effect of lithium on the products was not mentioned. STRATEN et al [18] found that $Li^+$ ion accelerated the precipitation rate of bayerite and promoted transformation of pseudoboehmite to bayerite in an extremely diluted sodium aluminate solution ($c$(Al)=4×10$^{-4}$ mol/L) containing lithium ion at 25−50 °C, and $LiAl_2(OH)_7{\cdot}2H_2O$ was formed by the combination of $Li^+$ and $Al(OH)_4^-$ in the sodium aluminate solution. FRENKEL et al [19] observed that $Li^+$ ion modified the structure of pseudoboehmite in the precipitation of aluminum hydroxide with adding NaOH into $AlCl_3$ solution containing lithium ion. To prepare alumina containing lithium, LI and LONG [20] believed that $Li^+$ ions in solution have no effect on precipitation rate and particle size distribution (PSD), and 80% lithium was co-precipitated in gibbsite precipitation. Therefore,

**Foundation item:** Project (2015BAB04B01) supported by the National Key Technology Research & Development Program of China; Project (CSUZC201811) supported by the Open-End Fund for the Valuable and Precision Instruments of Central South University, China

**Corresponding author:** Gui-hua LIU; Tel/Fax: +86-731-88830453; E-mail: liugh303@csu.edu.cn

DOI: 10.1016/S1003-6326(19)65039-9

the effect of lithium ion in solution on precipitation rate of ATH remains vague. Moreover, in addition to the increase in lithium content in ATH in the precipitation, the effect of lithium ion on PSD, morphology and crystallization of ATH remains unclear, all of which are related to alumina quality and subsequently directly involves in aluminum electrolysis.

To improve the quality of sandy alumina and to diminish the negative effects on aluminum electrolysis, the effects of lithium ion in solution on precipitation rate as well as lithium content, morphology and crystallization habit for ATH were investigated. Furthermore, the effect of $Li^+$ ion on gibbsite precipitation mechanism was also examined by analysis of PSD, X-ray diffractometry (XRD), X-ray photo-electron spectroscopy (XPS) and SEM.

## 2 Experimental

### 2.1 Materials

Aluminum hydroxide and sodium hydroxide (Aladdin Co., Ltd, 99.9%) were used to prepare sodium aluminate solutions with deionized water. Lithium aluminate (Wuhan 3B Science Co., 99%) was dissolved in sodium aluminate solution to obtain sodium aluminate solution containing lithium ion after filtration. Seed ATH assigned to gibbsite was received from Chalco. All chemicals used were of analytical grade.

### 2.2 Experimental procedures

Precipitation process was performed in a beaker (1000 mL) sealed by a plastic lid and heated by a water bath (±1 °C). Sodium aluminate solution containing lithium ion ($\rho(Na_2O)$=160.00 g/L, $\rho(Al_2O_3)$=181.54 g/L, $\rho(Li^+)$<0.5 g/L) and seed ATH were added into the beaker at 45−80 °C. Furthermore, 20 mL of the slurry was pumped out at a given time and then filtered with vacuum filtration. The solution (filtrate) was used to determine the concentration of $Na_2O$ and $Al_2O_3$. ATH (cake), washed three times with hot deionized water (about 95 °C), was used to determine lithium content, PSD, morphology, and phase compositions.

### 2.3 Methods

$Na_2O$ and $Al_2O_3$ concentrations (denoted by $c(Na_2O)$ and $c(Al_2O_3)$) in sodium aluminate solution were determined by titration [21]. Precipitation rate ($\eta$) was calculated according to the following equation:

$$\eta=(1-\alpha_{k,0}/\alpha_{k,t})\times100\% \quad (1)$$

where subscripts 0 and $t$ represent the initial stage and time $t$, respectively. $\alpha_k$ is defined as molar ratio of $Na_2O$ to $Al_2O_3$ in sodium aluminate solution.

Lithium content in ATH was determined by plasma emission spectroscopy (ICP-AES) (Intrepid II XSP, American Thermo). PSD was finished on Mastersizer 2000 (Malvern Instruments Ltd., UK). Surface element analysis was recorded on XPS (ESCALAB 250Xi, America Thermo Fisher). Particle image and phase were evaluated through scanning electron microscopy (SEM) (JSM−6360LV, Japan) and X-ray diffractometer (XRD) (Bruker, Germany), respectively.

Preferential orientation index $O$ suggests high degree of preferential orientation of crystal plane. $O$ value of ATH was calculated based on the XRD patterns according to the following equation [22]:

$$O=\frac{I_j/I_0}{\frac{1}{n}\sum_{j=1}^{n}(I_j/I_0)} \quad (2)$$

where $I_j$ and $I_0$ are the XRD intensity of the ($hkl$) plane in the experimental specimen (gibbsite) and the standard powder sample, respectively. $n$ is the number of planes.

To further elucidate the effect of lithium ion in solution on PSD of ATH, the particle number $N_i$ of each particle size range per unit volume (where $i$ ($i$=1, 2, 3, 4) represents <10 μm, 10–20 μm, 20–45 μm, and >45 μm, respectively) was calculated based on the data from the PSD curves of the seed ATH or ATH precipitated from solution containing lithium ion [23].

## 3 Results and discussion

### 3.1 Precipitation rate in sodium aluminate solution containing lithium ion

3.1.1 Effect of lithium ion concentration

Effect of lithium ion on the precipitation of ATH is often neglected because lithium ion concentration is remarkably low at low temperature [9]. Figure 1 shows the effect of lithium ion concentration on precipitation rate.

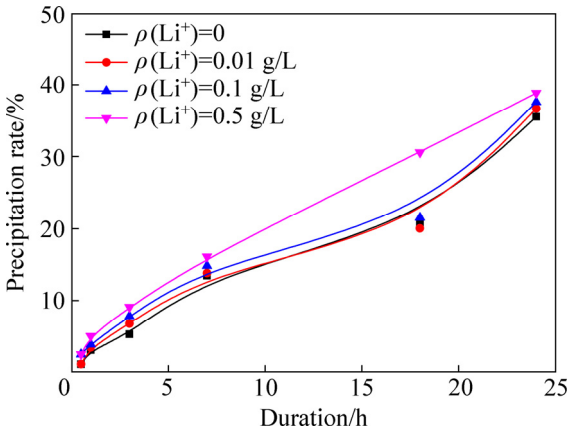


**Fig. 1** Effect of lithium ion concentration on precipitation rate ($\rho(Na_2O)$=160.00 g/L, $\rho(Al_2O_3)$=181.54 g/L, $T$=65 °C, seed ATH amount 100 g/L)

In Fig. 1, precipitation rate slightly increased with the increase in lithium ion concentration. The solution containing less than 0.1 g/L lithium achieved a slightly higher precipitation rate than the pure sodium aluminate solution. Increase in lithium concentration from 0.1 to 0.5 g/L further improved the precipitation rate particularly after 1 h. Results suggest that increase in lithium ion concentration favors the precipitation, which differs from results presented by LI and LONG [20].

3.1.2 Effect of temperature

Elevating temperature increases lithium solubility. However, high temperature decreases the precipitation rate due to the decrease in saturation of sodium aluminate solution. To simplify the precipitation process, a constant temperature was employed. Figure 2 presents the effect of temperature on precipitation rate in sodium aluminate solution containing lithium ion.

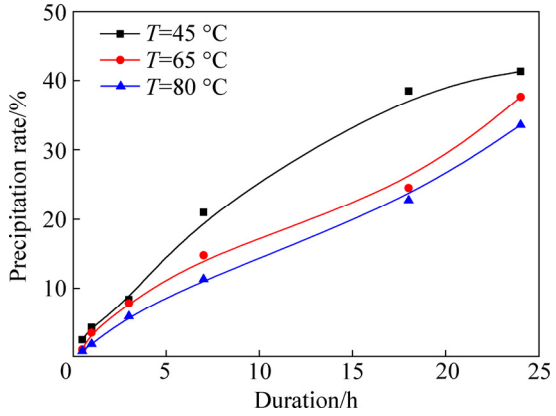


**Fig. 2** Effect of temperature on precipitation rate in sodium aluminate solution containing lithium ($\rho(Na_2O)$=160.00 g/L, $\rho(Al_2O_3)$=181.54 g/L; $\rho(Li^+)$=0.1 g/L; seed ATH amount 100 g/L)

As shown in Fig. 2, elevating temperature reduced the precipitation rate in aluminate solution containing lithium ion, which is in good agreement with results in the pure sodium aluminate solution [24].

In summary, lithium ion in solution affects the ATH precipitation. This suggests that much meaningful information will be obtained in subsequent discussion about variation of lithium content in ATH, and PSD, XRD, and morphology of ATH.

### 3.2 Lithium content in ATH precipitated from sodium aluminate containing lithium ion

3.2.1 Effect of lithium ion concentration

LI and LONG [20] proved that 80% lithium can be readily co-precipitated into ATH in the preparation of alumina containing lithium by digesting lithium-bearing minerals into aluminate solution. However, the effect of lithium ion concentration in solution on lithium content in ATH precipitated from solution remains unclear. Table 1 gives the variations of lithium content in ATH precipitated from different solutions.

**Table 1** Effect of lithium ion concentration in sodium aluminate solution on lithium content in ATH

| Duration/h | Lithium content in ATH/wt.% | | |
|---|---|---|---|
| | $\rho(Li^+)$=0.01 g/L | $\rho(Li^+)$=0.1 g/L | $\rho(Li^+)$=0.5 g/L |
| 0.083 | 0.0097 | 0.0331 | 0.0262 |
| 0.16 | 0.0106 | 0.0409 | 0.0545 |
| 0.5 | 0.0137 | 0.0408 | 0.0462 |
| 1 | 0.0191 | 0.0429 | 0.0466 |
| 3 | 0.0217 | 0.0515 | 0.0467 |
| 7 | 0.0195 | 0.0502 | 0.0470 |
| 18 | 0.0170 | 0.0441 | 0.0683 |
| 24 | 0.0174 | 0.0431 | 0.0687 |

$\rho(Na_2O)$=160.00 g/L, $\rho(Al_2O_3)$=181.54 g/L, $T$=65 °C, seed ATH amount 100 g/L, lithium content in seed 0.0076%

In Table 1, increasing lithium ion concentration improved lithium content in ATH, mainly due to the solubility of lithium ion in solution. However, increase in lithium content in ATH was not proportional to the lithium ion concentration. In addition, extending time slightly benefitted the lithium co-precipitated from solution of $\rho(Li^+)$=0.1 g/L and $\rho(Li^+)$=0.5 g/L.

To further illustrate lithium precipitation in various solutions, mass fraction of lithium precipitation was then calculated based on data in Table 1 and mass of ATH precipitated from solution based on data from Fig. 1. Results can be seen in Fig. 3.

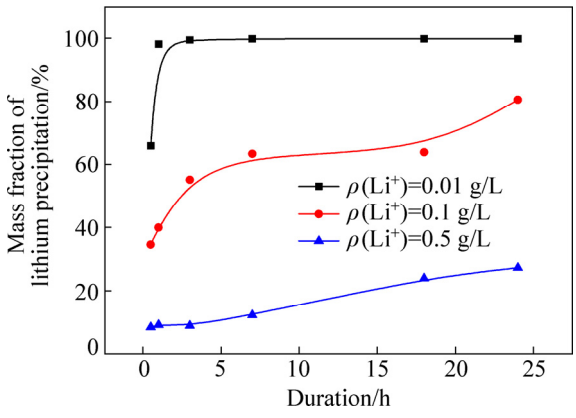


**Fig. 3** Effect of Li ion concentration in solution on mass fraction of lithium precipitation ($\rho(Na_2O)$=160.00 g/L, $\rho(Al_2O_3)$=181.54 g/L, $T$=65 °C, seed ATH amount 100 g/L, Li content in seed ATH 0.0076%)

As presented in Fig. 3, when the duration became long, the mass fraction of lithium precipitation quickly reached the maximum and remained almost constant in the solution of $\rho(Li^+)$=0.01 g/L possibly due to the adsorption of fresh ATH [25]. Meanwhile, the mass

fraction of lithium precipitation raised slowly in solution of $\rho(Li^+)$=0.5 g/L. Results also suggest that increasing lithium ion concentration reduced the mass fraction of lithium precipitation. This result differs from that deduced from the solubility of lithium aluminate hydrate [17], possibly due to the metastability of lithium ion in the supersaturate sodium aluminate solution and cake (ATH) washed with hot water, or the crystal form of aluminum hydroxide precipitated from sodium aluminate solution [26]. The reason will be explained in the further investigation.

3.2.2 Effect of temperature

Table 2 gives the influence of temperature on lithium precipitation rate.

Elevating the temperature (Table 2) inhibited the lithium precipitation and reduced the lithium content in ATH. The higher the temperature was, the lower the lithium content was in ATH at early precipitation stage. In addition, the mass fraction of lithium precipitation decreased with elevating temperature based on the data in Table 2 and ATH mass precipitated from solution in Fig. 2. For example, the mass fractions of lithium precipitation after 18 h were 61.62%, 55.76% and 39.99% at 45 °C, 65 °C and 80 °C, respectively.

**Table 2** Effect of temperature of seed precipitation process on lithium content in ATH

| Duration/h | Lithium content in ATH/wt.% | | |
|---|---|---|---|
| | $T$=45 °C | $T$=65 °C | $T$=80 °C |
| 0.083 | 0.0322 | 0.0331 | 0.0150 |
| 0.16 | 0.0379 | 0.0409 | 0.0141 |
| 0.5 | 0.0349 | 0.0408 | 0.0206 |
| 1 | 0.0372 | 0.0429 | 0.0347 |
| 3 | 0.0405 | 0.0515 | 0.0360 |
| 7 | 0.0499 | 0.0502 | 0.0381 |
| 18 | 0.0322 | 0.0441 | 0.0327 |
| 24 | 0.0351 | 0.0431 | 0.0366 |

$\rho(Na_2O)$=160.00 g/L, $\rho(Al_2O_3)$=181.54 g/L, $\rho(Li^+)$=0.1 g/L, seed ATH amount 100 g/L, Li content in ATH seed 0.0076%

Therefore, lithium was readily precipitated from solution containing lithium ion, which led to the rich-lithium alumina followed calcining rich-lithium ATH. The removal of lithium ion from solution or elevating temperature can reduce the lithium content in ATH.

### 3.3 PSD of ATH precipitated from sodium aluminate solution containing lithium ion

3.3.1 Effect of time

The fine ATH is generally attributed to the concentrated solution ($\rho(Na_2O)$≥160 g/L), vigorous stirring, sodium oxalate, rapid precipitation or high precipitation rate. Attention is scarcely paid to the effect of lithium ion in solution. PSD curves of ATH are shown in Fig. 4.

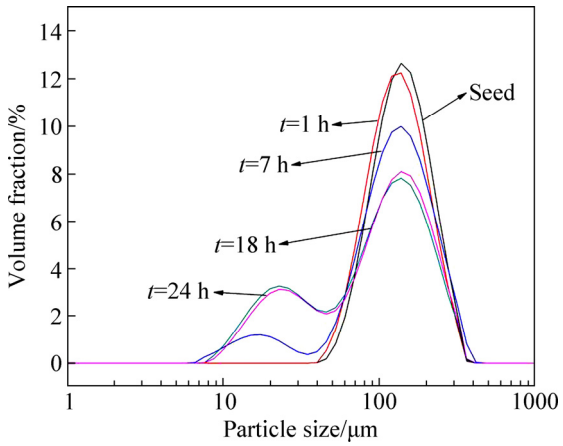


**Fig. 4** Effect of time on PSD of ATH ($\rho(Na_2O)$=160.00 g/L, $\rho(Al_2O_3)$=181.54 g/L, $T$=65 °C, $\rho(Li^+)$=0.1 g/L, seed ATH amount 100 g/L)

Figure 4 showed that, when precipitation occurred in sodium aluminate solution containing lithium ion, a new peak of the fine particle (<30 μm) was observed. The finding suggests that lithium ion in solution promotes the fine ATH precipitation. Moreover, extending time generated a large amount of the fine ATH because of the remarkable increase in the intensity of the peak for the fine particle. By contrast, the peak intensity at 60–120 μm correspondingly decreased along with increasing half-width of the peak. The fact confirms that lithium ion in the solution is unfavorable in precipitation of the coarse ATH.

The fine particle, less than 45 μm, is detrimental to aluminum electrolysis, while the finer particle (<20 μm) promotes the precipitation and is preferentially agglomerated in precipitation process. Therefore, the particle size of ATH was then categorized into four ranges (0−10 μm, 10−20 μm, 20−45 μm, and >45 μm) to further discuss the variation in particle size. Results can be seen in Fig. 5.

As shown in Fig. 5, the total particle number increased significantly in the early stage (1−15 h) and then decreased slowly. Meanwhile, the particle number in each particle size range varied differently. For example, the particle number at 0−10 μm initially remarkably increased and decreased rapidly thereafter. The particle number at 10−20 μm also initially remarkably increased, and then decreased slowly. However, the coarse particle number at >45 μm decreased slightly. Therefore, a large number of the fine particles (<20 μm) occurred in the early precipitation stage (<15 h), mainly attributed to the remarkable nucleation and slight agglomeration. Furthermore, the

fine ATH, together with the seeds, improves the precipitation rate after 1 h in the precipitation (Fig. 1) due to a large amount of the specific surface area from the fine particle.

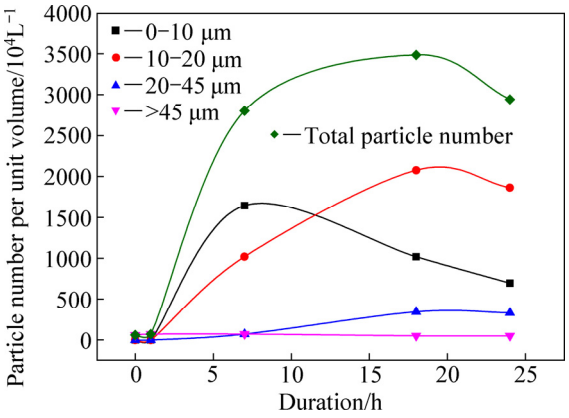


**Fig. 5** Variation in ATH in each particle size range during precipitation ($\rho(Na_2O)$=160.00 g/L, $\rho(Al_2O_3)$=181.54 g/L, $T$=65 °C, $\rho(Li^+)$=0.1 g/L, seed ATH amount 100 g/L)

3.3.2 Effect of lithium ion concentration

The effect of lithium ion concentration on PSD and particle number can be seen in Fig. 6 and Table 3, respectively.

Figure 6 showed that a peak associated with fine particles at 5−40 μm was observed. Increase in lithium ion concentration shifted the peak at 5−40 μm toward the fine particle. Simultaneously, the peak intensity of the coarse particle at 60−120 μm decreased. The observations confirm that increase in lithium ion concentration generates the fine particles. Table 3 indicated that the fine particles number at 0−20 μm significantly increased as lithium ion concentration increased. Furthermore, the number of superfine particles with size of 0−10 μm notably raised in solution of $\rho(Li^+)$=0.5 g/L, which was approximately 331 times greater than that in solution of $\rho(Li^+)$=0.01 g/L. The remarkable occurrence of the fine particles also suggests that increasing the lithium ion concentration will significantly promote the nucleation of ATH in precipitation.

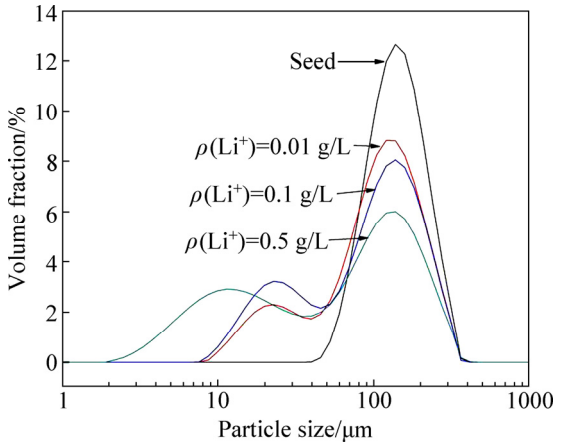


**Fig. 6** Effect of lithium ion concentration on PSD of ATH ($\rho(Na_2O)$=160.00 g/L, $\rho(Al_2O_3)$=181.54 g/L, $T$=65 °C, $t$=24 h, seed ATH amount 100 g/L)

3.3.3 Effect of temperature

Elevating temperature is often adopted to eliminate the fine particle by agglomeration. Table 4 and Fig. 7 show the effect of temperature on PSD of ATH.

Figure 7 indicated that elevating temperature dropped the peak intensity at 10−40 μm, whereas increased the peak intensity at 60−120 μm. However, there existed a peak for particle size less than 30 μm at 80 °C. The fact implies elevating temperature cannot eliminate the fine particle in solution of $\rho(Li^+)$=0.1 g/L. As shown in Table 4, the increase in temperature considerably decreased the number of fine particles (0−45 μm) and slightly increased the number of coarse particles (>45 μm). For example, the number of fine particles in 0−10 μm at 80 °C decreased compared with that at 45 °C. Therefore, lithium ion in solution should be removed, although elevating temperature can diminish some fine particle.

**Table 3** Effect of $Li^+$ concentration on particle number in each particle size range

| Li ion concentration/(g·L$^{-1}$) | Particle number/$10^4$ L$^{-1}$ | | | | |
|---|---|---|---|---|---|
| | 0−10 μm | 10−20 μm | 20−45 μm | >45μm | Total |
| 0.01 | 298.58 | 1294.17 | 216.25 | 61.47 | 1870.47 |
| 0.1 | 694.63 | 1872.70 | 341.49 | 50.68 | 2959.50 |
| 0.5 | 99066.63 | 2471.98 | 220.47 | 44.43 | 101803.51 |

**Table 4** Effect of temperature on particle number in each particle size range

| Temperature/°C | Particle number/$10^4$ L$^{-1}$ | | | | |
|---|---|---|---|---|---|
| | 0−10 μm | 10−20 μm | 20−45 μm | >45 μm | Total |
| 45 | 1490800 | 3830.47 | 526.34 | 39.05 | 1495195.88 |
| 65 | 819.54 | 1962.51 | 352,96 | 52.00 | 3187.01 |
| 80 | 1616.51 | 814.58 | 69.34 | 67.21 | 2567.64 |

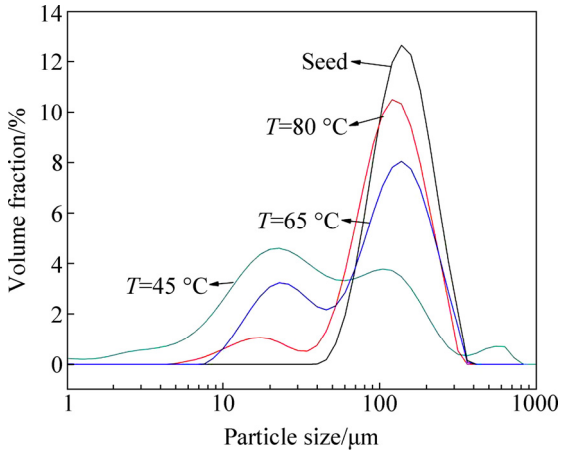


**Fig. 7** Effect of temperature on PSD of ATH precipitated from solution containing lithium ion ($\rho(Na_2O)$=160.00 g/L, $\rho(Al_2O_3)$=181.54 g/L, $\rho(Li^+)$=0.1 g/L, $t$=24 h, seed ATH amount 100 g/L)

### 3.4 Morphology of ATH precipitated from sodium aluminate solution containing lithium ion

Above results confirmed that the presence of lithium ion in solution led to the precipitation of the fine ATH and increased the precipitation rate. The morphology of ATH precipitated from the solution containing lithium ion may provide some supplementary explanation. Figure 8 shows the morphologies of ATH precipitated from sodium aluminate solutions containing lithium ion.

In Fig. 8, few fine particles were attached on the surface of the coarse particle for seed ATH (Figs. 8(a, b)). However, lithium ion in the solution changed the morphology of ATH precipitated from sodium aluminate solution (Figs. 8(c−f)). A large number of the fine bar- or flake-shaped particles were attached on the surface of the coarse particles in addition to the fine particle scattering around the coarse particle. This shape is distinct from the hexangular rod-like ATH precipitated from the sodium

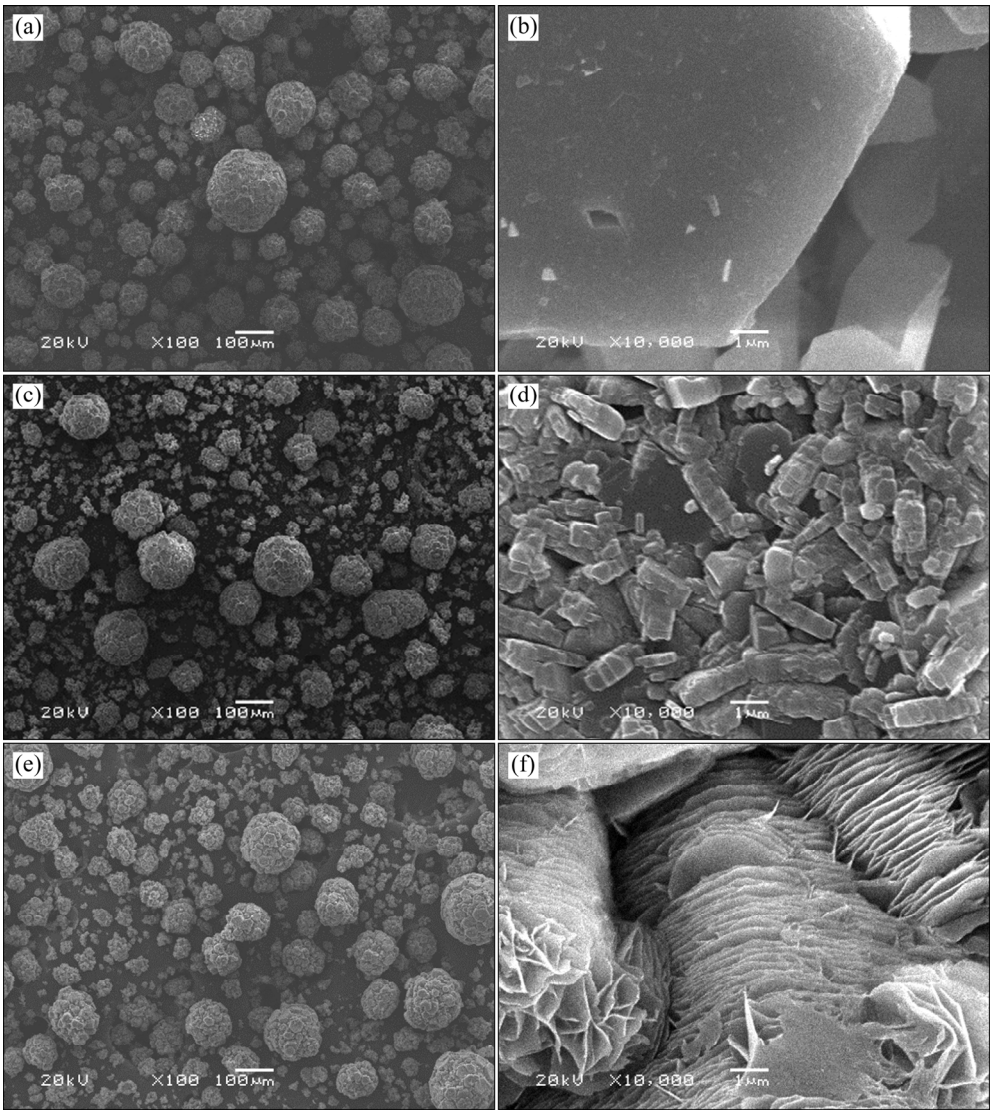


**Fig. 8** Effect of lithium ion concentration on morphology of seed ATH (a, b), ATH precipitated from solution containing 0.1 g/L (c, d) and 0.5 g/L (e, f) $Li^+$ after 3 h ($\rho(Na_2O)$=160.00 g/L, $\rho(Al_2O_3)$=181.54 g/L, $T$=45 °C, seed ATH amount 100 g/L)

aluminate solution [27−29]. Furthermore, the fine particles attached on the coarse particles will easily fall down due to particle collision in fluid (called as the secondary nucleation) with ATH seed over 300 g/L, thereby generating numerous fine particles as mentioned in Figs. 4, 6 and 7. Moreover, a large amount of bar- or flake-shaped particles attached on the coarse particles also weaken alumina strength followed by calcining as-precipitated ATH. This poor strength for alumina also negatively affects aluminum electrolysis.

### 3.5 XRD and XPS for ATH precipitated from sodium aluminate solution containing lithium ion

Figures 9 and 10 display the XRD patterns and XPS of ATH precipitated from the solution containing lithium ion, respectively.

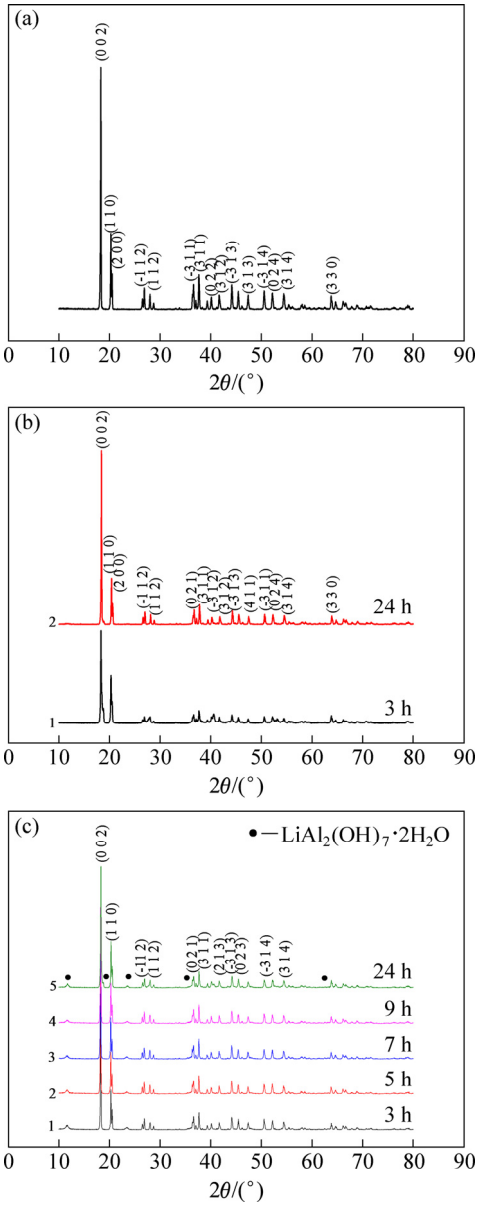


**Fig. 9** XRD patterns of seed ATH (a), ATH from solution containing 0.1 g/L (b) and 0.5 g/L (c) $Li^+$

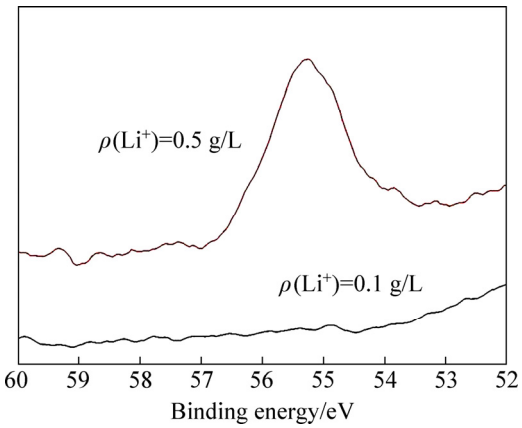


**Fig. 10** XPS patterns of ATH from solution containing 0.1 and 0.5 g/L $Li^+$

Like gibbsite in seed ATH (Fig. 9(a)), gibbsite instead of bayerite [6,19] was precipitated from the concentrated sodium aluminate solution containing lithium ion, as shown in Figs. 9(b, c). In addition, $LiAl_2(OH)_7·2H_2O$ was barely detectable in the solution of $\rho(Li^+)\leq 0.1$ g/L. However, a few $LiAl_2(OH)_7·2H_2O$ was observed in the solution of $\rho(Li^+)=0.5$ g/L (Fig. 9(c)). Meanwhile, XPS results showed that characteristic peaks assigned to Li were found in the solution of $\rho(Li^+)=0.5$ g/L (Fig. 10). The contents of Al and Li on ATH surface in solution of $\rho(Li^+)=0.5$ g/L were 19.69% and 4.15%, respectively. These results acquired from the solution of $\rho(Li^+)\leq 0.1$ g/L confirm that lithium ion in solution affects the nucleation of gibbsite.

Results in Fig. 9 also indicated that the diffraction intensities corresponding to various planes of gibbsite varied differently. Therefore, the preferential orientation index $T$ of each crystal plane of gibbsite precipitated in 3−24 h was calculated based on the XRD patterns (Tables 5 and 6).

High value of $T$ represents high degree of preferential orientation. Relative to the preferential (001) plane of gibbsite from sodium aluminate solution [30,31], the preferential orientation index $T$ of the (110) and (200) planes for gibbsite from the solution containing lithium was found after 3 h or 24 h (Tables 5 and 6). The preferential growth of the (110) and (200) plane on the surface of seed gibbsite might produce the fine particles with bar or flake shape (Figs. 8(c−f)). Meanwhile, it seems that lithium ion in solution determines nucleation and is related to the growth of crystal plane. The finding suggests that lithium ion does not intercalate in gibbsite by occupying vacant positions of gibbsite [32,33], which occurred in lithium-bearing solution ($LiNO_3$, LiCl, LiBr, LiI and $Li_2SO_4$) with the addition of gibbsite into solution.

**Table 5** Preferential orientation index $T$ of each plane of ATH precipitated from solution containing 0.1 g/L $Li^+$

| Duration/h | Preferential orientation index, $T$ | | | | | | | |
|---|---|---|---|---|---|---|---|---|
| | (002) | (110) | (200) | (112) | (202) | (021) | (311) | (024) |
| 0 | 0.679 | 1.327 | 1.230 | 1.035 | 0.565 | 0.865 | 1.204 | 0.896 |
| 3 | 0.899 | 1.495 | 1.327 | 1.282 | 0.660 | 0.551 | 1.270 | 0.989 |
| 24 | 0.643 | 2.083 | 1.841 | 1.126 | 0.472 | 0.748 | 1.013 | 0.823 |

Sample at 0 h was ATH seed

**Table 6** Preferential orientation index $T$ of each plane of ATH precipitated from solution containing 0.5 g/L $Li^+$

| Duration/h | Preferential orientation index, $T$ | | | | | | | |
|---|---|---|---|---|---|---|---|---|
| | (002) | (110) | (200) | (112) | (202) | (021) | (311) | (024) |
| 0 | 0.679 | 1.327 | 1.230 | 1.035 | 0.565 | 0.865 | 1.204 | 0.896 |
| 3 | 0.780 | 1.312 | 1.337 | 0.937 | 0.624 | 0.829 | 1.112 | 0.952 |
| 24 | 0.706 | 1.698 | 1.544 | 1.041 | 0.541 | 0.767 | 1.120 | 0.861 |

Sample at 0 h was ATH seed

## 4 Conclusions

(1) Lithium ion in sodium aluminate solution improved the precipitation rate and slightly increased the lithium content in ATH. The mass fraction of lithium precipitates reduced with the increase in lithium ion concentration. Elevating temperature decreased the precipitation rate and lithium content in ATH. Lithium aluminate hydrate was barely found in ATH in solution of $\rho(Li^+)\leq 0.1$ g/L.

(2) ATH precipitated from the sodium aluminate solution containing lithium ion was identified as gibbsite. Lithium in the solution promoted the formation of fine particles and increased in the total particle number due to the preferential nucleation (or secondary nucleation). Furthermore, the presence of lithium ion significantly changed the morphology of gibbsite. The (110) and (200) planes of gibbsite grew preferentially, rather than (001) plane in solution free of lithium. A large number of fine bar- or flake-shaped particles were attached on the coarse particle of ATH, benefitting the formation of the fine particle and reducing the strength of alumina.

## References

[1] BORDERIE B, BASUTCU M, BARRANDON J N, PINAULT J L. Accurate determination of lithium, boron, fluorine and sodium in some matrices using low energy alpha-particles induced gamma-rays [J]. Journal of Radioanalytical Chemistry, 1980, 56(1−2): 185−198.

[2] LIU Xiao-ming, RUDNICK R L, MCDONOUGH W F, CUMMINGS M L. Influence of chemical weathering on the composition of the continental crust: Insights from Li and Nd isotopes in bauxite profiles developed on Columbia River Basalts [J]. Geochimica et Cosmochimica Acta, 2013, 115(5): 73−91.

[3] SUN Yu-zhuang, ZHAO Cun-liang, LI Yan-heng, LIU Shi-ming. Li distribution and mode of occurrences in Li-bearing coal seam #6 from the Guanbanwusu Mine, Inner Mongolia, Northern China [J]. Energy Exploration & Exploitation, 2012, 30(1): 109−130.

[4] TOURTELOT H A, BRENNER-TOURTELOT E F. Lithium, a preliminary survey of its mineral occurrence in flint clay and related rock types in the United States [J]. Energy, 1978, 3(3): 263−272.

[5] GOMES H I, MAYES W M, ROGERSON M, STEWART D I, BURKE I T. Alkaline residues and the environment: A review of impacts, management practices and opportunities [J]. Journal of Cleaner Production, 2016, 112(4): 3571−3582.

[6] LV Xiao-jun, SHUANG Ya-jing, LI Jie, CHEN Shi-yue, LAI Yan-qing, ZHANG Hong-liang, LIU Ye-xiang. Physicochemical properties of industrial aluminum electrolytes enriching Li and K: The liquidus temperature [J]. Metallurgical & Materials Transactions B, 2017, 48(2): 1315−1320.

[7] LV Xiao-jun, CHEN Shi-yue, LAI Yan-qing, ZHANG Hong-liang, LI Jie, TIAN Zhong-liang. Effect of $LiAlO_2$ and KF on physicochemical properties for industrial aluminum electrolyte [J]. TMS Light Metals, 2016: 705−709.

[8] MORISHIGE T, HAARBERG G M, GUDBRANDSEN H, SKYBAKMOEN E, SOLHEIM A, TEKENAKA T. Effects of composition and temperature on current efficiency for aluminium electrolysis from cryolite-based molten alumina electrolytes [J]. ECS Transactions, 2017, 77(11): 997−1002.

[9] VILYUGINA M D, MAKARENKOV V M, EREMIN N I. Lithium oxide solubility in aluminate solutions at elevated temperatures [J]. Izvestiya Vysshikh Uchebnykh Zavedenii, Tsvetnaya Metallurgia, 1983, 5: 72−74. (in Russian)

[10] LIU Gui-hua, LI Xiao-bin, ZHANG Chuan-fu, PENG Zhi-hong, HE Bo-quan. Formation and solubility of potassium aluminosilicate [J]. Transactions of the Nonferrous Metals Society of China, 1998, 8(1): 120−122.

[11] LOH J S C, WALTING H R, PARKINSON G M. Alkali cations−Roles and effect on gibbsite crystallization [J]. TMS Light Metals, 2001: 127−133.

[12] CHEN Jin-qing, LIU Ji-bo, ZHANG Ping-min, YIN Zhou-lan, CHEN Qi-yuan, ZHANG Yu-min. Precipitation rate and particle size distribution of seed precipitation proceeding in sodium and potassium aluminate solutions [J]. Chinese Journal of Nonferrous Metals, 2004, 14(3): 515−519. (in Chinese)

[13] XIE Yan-li, ZHAO Qun, LU Zi-jian, JIN Zhe-nan, BI Shi-wen. Study on negative effect of $K_2O$ on precipitation of gibbsite [J]. TMS Light Metals, 2005: 219−222.

[14] XIE Yan-li, ZHAO Qun, JIN Zhe-nan, LU Zi-jian, BI Shi-wen. Study on the effect of $K_2O$ on seed precipitation in sodium aluminate liquors [J]. TMS Light Metals, 2006: 159−163.

[15] LI Jun, PRESTIDGE C A, ADDAI-MENSAH J. The influence of alkali metal ions on homogeneous nucleation of $Al(OH)_3$ crystals from supersaturated caustic aluminate solutions [J]. Journal of Colloid and Interface Science, 2000, 224(2): 317−324.

[16] LEE M Y, ROHL A L, GALE J D, LINCOLN F J. The influence of metal ion inclusion on the morphology of gibbsite [J]. Chemical Engineering Research and Design, 1996, 74(7): 739−743.

[17] XU Xin, ZHOU You, FAN Mao-hong, LV Zi-jian, TANG Yang, SUN Yan-zhi. Lithium adsorption performance of a three-dimensional porous $H_2TiO_3$-type lithium ion-sieve in strong alkaline Bayer liquor [J]. RSC Advances, 2017, 7(31): 18883−18891.

[18] STRATEN H A V, SCHOONEN M A A, BRUYN P L D. Precipitation from supersaturated aluminate solutions. III. Influence of alkali ions with special reference to $Li^+$ [J]. Journal of Colloid and Interface Science, 1985, 103(2): 493−507.

[19] FRENKEL M, GLASNER A, SARIG S. Crystal modification of freshly precipitated aluminum hydroxide by lithium ion intercalation [J]. Chemischer Informationsdienst, 1980, 11(23): 507−510.

[20] LI Xiao-bin, LONG Yuan-zhi. Studies of the process for producing lithium-bearing alumina [J]. Mining and Metallurgical Engineering, 1989, 9(3): 46−50. (in Chinese)

[21] LIU Gui-hua, LI Zheng, QI Tian-gui, ZHOU Qiu-sheng, PENG Zhi-hong, LI Xiao-bin. Continuous changes in electrical conductivity of sodium aluminate solution in seeded precipitation [J]. Transactions of Nonferrous Metals Society of China, 2015, 25(12): 4160−4166.

[22] ZHAO Hai-jun, LIU Lei, WU Ya-ting, HU Wen-bin. Investigation on wear and corrosion behavior of Cu–graphite composites prepared by electroforming [J]. Composites Science and Technology, 2007, 67(6): 1210−1217.

[23] ZHOU Qiu-sheng, PENG Dian-jun, PENG Zhi-hong, LIU Gui-hua, LI Xiao-bin. Agglomeration of gibbsite particles from carbonation process of sodium aluminate solution [J]. Hydrometallurgy, 2009, 99(3): 163−169.

[24] ZHANG Ying, ZHENG Shi-li, DU Hao, XU Hong-bin, WANG Shao-na, ZHANG Yi. Improved precipitation of gibbsite from sodium aluminate solution by adding methanol [J]. Hydrometallurgy, 2009, 98(1): 38−44.

[25] LEE J M, BAUMAN W C. Removal of sulfate ions from brine using amorphous polymeric zirconium oxide formed within a macroporous polymer matrix. US4415678 [P]. 1983−11−15.

[26] KUANG Ge, LI Huan, HU Song, JIN Ran, LIU Shan-jun, GUO Hui. Recovery of aluminium and lithium from gypsum residue obtained in the process of lithium extraction from lepidolite [J]. Hydrometallurgy, 2015, 157: 214−218.

[27] JOSHI U A, LEE J S. Large-scale, surfactant-free, hydrothermal synthesis of lithium aluminate nanorods: Optimization of parameters and investigation of growth mechanism [J]. Inorganic Chemistry, 2007, 46(8): 3176−3184.

[28] HU Lin-feng, QIAO Bin, TANG Zi-long, ZHANG Zhong-tai. Hydrothermal routes to various controllable morphologies of nanostructural lithium aluminate [J]. Materials Research Bulletin, 2007, 42(8): 1407−1413.

[29] HU Lin-feng, TANG Zi-long, ZHANG Zhong-tai. Hydrothermal synthesis of single crystal mesoporous $LiAlO_2$, nanobelts [J]. Materials Letters, 2008, 62(12): 2039−2042.

[30] FREIJ S J, PARKINSON G M, REYHANI M M. Direct observation of the growth of gibbsite crystals by atomic force microscopy [J]. Journal of Crystal Growth, 2004, 260(1): 232−242.

[31] FU Weng, VAUGHAN J, GILLESPIE A. In situ AFM investigation of gibbsite growth in high ionic strength, highly alkaline, aqueous media [J]. Hydrometallurgy, 2016, 161: 71−76.

[32] ISUPOV V P, GABUDA S P, KOZLOVA S G, CHUPAKHINA L É. Structural mechanism of selective binding of lithium on a solid matrix of $Al(OH)_3$, from aqueous solutions [J]. Journal of Structural Chemistry, 1998, 39(3): 362−366.

[33] GARETH R W, DERMOT O H. A kinetic study of the intercalation of lithium salts into $Al(OH)_3$ [J]. Journal of Physical Chemistry B, 2006, 110(22): 10619−10629.

# 铝酸钠溶液中锂离子对溶液种分的影响

黄文强，刘桂华，剧锦斌，李小斌，周秋生，齐天贵，彭志宏

中南大学 冶金与环境学院，长沙 410083

**摘　要：**研究锂离子对铝酸钠溶液分解率和氢氧化铝的锂含量、形貌和结晶习性的影响。结果表明，随着溶液中锂离子浓度的增加，溶液的分解率和氢氧化铝中锂含量均增大，而溶液中锂析出的质量分数减小。溶液中锂离子的存在使得氢氧化铝优先成核(或二次成核)而产生更多细小的颗粒，导致溶液中总粒子数显著增多。升高温度或减小溶液中锂离子浓度可减小氢氧化铝中锂浓度和减少细粒子数。此外，溶液中锂离子促进三水铝石(110)和(200)晶面的优先生长，导致大量细棒状和片状氢氧化铝附着在粗粒上，并促进成核，这将导致氧化铝强度的降低。研究结果将为提高氧化铝质量提供指导作用。

**关键词：**锂；铝酸钠；种分；氢氧化铝

**(Edited by Bing YANG)**